batteries

MDPI

Article

Revisiting Pulse-Based OCV Incremental Capacity Analysis for Diagnostics of Li-Ion Batteries

Julia Wind and Preben J. S. Vie *

Institute for Energy Technology (IFE), NO-2007 Kjeller, Norway; julia.wind@ife.no
* Correspondence: preben.vie@ife.no

Abstract: This paper presents the concept of applying incremental capacity analysis (ICA) on the OCV curve in the SoC space. The OCV curve can be obtained from any sequence of discharge or charge current or power pulse with a necessary rest period to allow the cell to reach a pseudo-OCV after each pulse. With a high resolution (>100 pulses) in the full SoC window, an OCV-vs.-SoC curve can be obtained with sufficient accuracy to perform an ICA on the obtained OCV curve. ICA as a diagnostic technique has commonly been applied on Li-ion cells with constant charge and discharge at slow currents. However, a slow controlled constant current charge or discharge is normally not feasible and cannot be easily applied to a battery in an application. Here, we revisit pulse-based ICA to supplement the conventional constant-current-based technique. Based on actual ageing data, we show that ICA performed on a selection of high-resolution OCV curves is comparable or better than conventional ICA with constant current. The main advantage of OCV-ICA is that it can be applied to most cells and systems without a significant interruption of normal cell operation. OCV-ICA can provide valuable insights into ageing mechanisms as well as, e.g., detailed information on changes in internal resistance.

Keywords: Li-ion battery; diagnostics; ICA; dQ/dV; OCV; battery system; aging; SoH; SoS

Citation: Wind, J.; Vie, P.J.S. Revisiting Pulse-Based OCV Incremental Capacity Analysis for Diagnostics of Li-Ion Batteries. *Batteries* **2024**, *10*, 277. https://doi.org/10.3390/batteries10080277

Academic Editor: Dino Tonti

Received: 24 June 2024
Revised: 30 July 2024
Accepted: 31 July 2024
Published: 3 August 2024

1. Introduction

The Li-ion battery (LIB) has become the most popular rechargeable battery since its commercial introduction in the 1990s. It was originally used as a battery in consumer electronics and was later introduced as the energy battery of electric vehicles (EVs) when, e.g., the Nissan Leaf and Mitsubishi i-MiEV were introduced in 2010 and 2009. Later, the LIB has entered the market in both electric energy storage (ESS) [1] applications and large electric and hybrid electric ships [2]. The LIB is still the most used rechargeable battery due to its superior energy density and efficiency compared to most other rechargeable batteries.

However, LIBs are more prone to fires than other batteries. This is due to their inherent higher energy density as well as the flammability of, especially, anode materials, separator, and electrolyte solvents. In addition, ageing and degradation can considerably contribute to decreasing the safety of a LIB [3]. A LIB can age in several ways. The effects of different ageing mechanisms are commonly classified into different ageing modes, such as loss of lithium inventory (LLI), loss of active material (LAM), and impedance increase due to reaction kinetics degradation [4].

One degradation mechanism leading to LLI that will significantly impact the battery safety is irreversible lithium plating. During lithium plating, metallic lithium forms on the anode surface [5]. This happens specifically when charging at too high currents and low temperatures (<10 °C). Recent reports have shown that this can already happen at moderate temperatures (15–25 °C) and currents [6]. Metallic lithium can in the worst case create a short circuit in the battery cell and cause a fire and or explosion. More commonly, metallic lithium will not short the battery but will remain within the anode, contributing to accelerated degradation as well as being a potential future safety hazard. Especially

when a battery has aged, the path of ageing can considerably affect the safety properties of the battery and cause dramatic differences in the severity of a possible safety incident. While battery safety tests are routinely performed on new cells, the understanding and experimental assessment of the state of safety (SoS) of aged cells in general and of cells aged under different conditions is still scarce [7]. Consequently, the SoS is commonly assumed to be directly related to the battery's state of health (SoH), and its monitoring is performed to avoid the further use of LIBs that may have aged in a detrimental fashion and can pose an increased fire safety risk.

Several techniques for battery SoH monitoring exist [8]. These encompass, e.g., a simple measurement of remaining capacity, DC resistance monitoring, or more elaborate methodologies such as electrochemical impedance spectroscopy (EIS) [9], intermittent current interrupt (ICI) [10], high-power pulse characterization (HPPC) [8], incremental capacity analysis (dQ/dV, ICA) [11], differential voltage analysis (dV/dQ, DVA) [12], and entropy spectroscopy [13]. While some of these methods only yield very basic information on the battery's SoH, others might give insight into how the battery has aged and through which mechanisms this has happened. From an applied perspective, the ICA and DVA methodologies may be the most versatile diagnostic methods, as they only require a constant low current of the Li-ion cell. Detailed analysis of the obtained IC and DV curves can then reveal correlations between capacity loss and degradation and thus allow for a more detailed assessment of the battery's SoH and, potentially, also of the battery's SoS [7]. The ICA technique and its applicability have been thoroughly described in the literature [4,8,11,14–17]. However, obtaining the full constant-current (dis)charge of the battery required for ICA can be challenging and is not feasible during the actual battery operation. Due to the commonly uncertain and incomplete charging and discharge conditions in addition to the quite sparse constant-current periods in real-world applications, significant and challenging data-preprocessing is necessary to obtain usable IC data [16].

The open-circuit voltage (OCV) curve is frequently used as a reference in battery modelling and SoC estimations in battery manage systems (BMS) [18]. The OCV is the stable thermodynamic state of a battery in any state of charge (SoC), representing the change in reversible Gibbs free energy of the anode and cathode reactions. The OCV is measured when there is no current in the battery and the battery voltage has stabilized to a "constant value". However, OCV relaxation is an asymptotic process and will only approach, but not actually reach, the "true" OCV value. This means that there is no constant OCV, but typically, a pseudo-OCV is assumed to have been reached after, e.g., 1 or 2 h of relaxation [8]. Consequently, the measurement of an OCV curve can be very time-consuming and not feasible on a regular basis. E.g., for an OCV curve with a SoC resolution of 1% and a relaxation time of one hour at each step, this would give a total of 204 h for a full OCV curve for both charge and discharge with C/2 current steps in between, summing up to more than 8 days for one full detailed OCV measurement. Quite commonly, the cell voltage of a slow discharge (<C/20) [11] or the average of slow charge and discharge curves [19] is used as a pseudo-OCV curve, still requiring >40 h of measurement time for a new cell. Several methods have been investigated to obtain a pseudo-OCV curve at reduced measurement times, as well as advanced methods for OCV reconstruction [20,21] to speed up the process even further. Note that within this work, we will use "pseudo-OCV" (pOCV) as a very general term for an approximation of OCV.

As opposed to constant-current (CC) measurements across the full SoC window, pOCV values can be considerably easier to obtain during actual battery operation within an application. In fact, the pOCV curve can be obtained from any sequence of discharge or charge current or power pulse with a necessary rest period to allow the cell to reach a pOCV after each pulse. This will allow for the establishment of a pOCV curve without a significant operational interruption. This OCV curve can be further used as input to an ICA, not requiring slow CC conditions but based on operational data as illustrated in Figure 1, obtaining an OCV-IC curve instead.

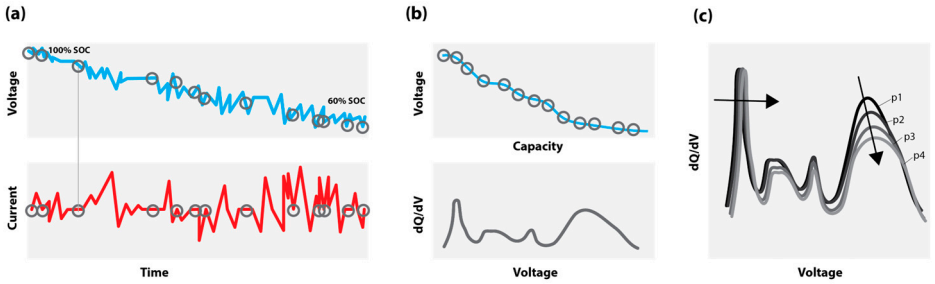

Figure 1. Illustration of the concept of OCV-ICA applied to operational data. pOCV data can be extracted from actual operational battery data with naturally occurring randomized current breaks (**a**); the pOCV curve is reconstructed from rest periods (upper), while the IC curve is then extracted from the pOCV curve (below) (**b**); changes in OCV-ICA due to ageing can then be compared (**c**).

The reconstruction of a battery's OCV curve is currently being used extensively for SoC estimation in battery systems [22]. However, its differentiation and, hence, potential analogy to common CC diagnostics have not been extensively explored in the literature. Already in 2013, Petzl et al. [18] directly compared continuous slow CC voltage profiles with incremental OCV curves for the establishment of a "fully relaxed OCV". IC and DV analyses on both CC and OCV measurements were used to check the quality of the obtained curves with respect to reproducing the main electrode features. Blanc [20] showed that the discharge OCV could be estimated with a fast model-based method within 10 h with a current pulse method without any rest periods. The estimated OCV curve was compared to a 25 h CC curve directly, and by comparing the corresponding IC-curves..

However, both Petzl and Blanc did not use the obtained differentiated pOCV curves for diagnostic purposes. Goldammer et al. [9] evaluated EIS data and the OCV curve for the identification of the degradation modes for a small set of aged cells and also briefly performed a DVA on the pOCV curves. To the best of our knowledge, no further research explored the application of OCV-ICA within the diagnostic assessment of battery ageing and its applicability to assess safety critical ageing conditions. The limited research on OCV-ICA is further confirmed in the extensive review paper on Li-ion cell characterization methods by Barai [8]. Barai et al. presented, e.g., methods to estimate pOCV curves through GITT measurements and discussed the literature on the low C-rate cycling applicability to both ICA and DVA but did not link the measurements of OCV curves and their derivative to DVA and ICA (see Table 1 in [8]).

With respect to online diagnostics, i.e., establishing degradation modes without operational interruption, Prosser et al. claimed to be the first, presenting their work on operando quantitative diagnostics [23] for identifying degradation modes based on measurements of temperatures, voltage, and current during operation.

In this paper, we revisit and elaborate on the OCV-ICA methodology. This is carried out by presenting a direct comparison between OCV-ICA and conventional CC-ICA, on an exemplary ageing dataset. We show that both methodologies can resolve qualitative diagnostic differences between different ageing temperatures. In addition, we explore methods to accelerate the measurements of pOCV curves with a focus on the needed quality of the OCV-IC curve compared to CC-IC curves obtained at slow C-rates (C/10 and C/20). This may allow for the ICA methodology to be extended through OCV-ICA to most cells and systems without a significant interruption of normal cell operation and consequently provide not only SoH estimations, but also valuable insights into the ageing mechanisms and detailed information on changes in internal resistance and state of safety.

To illustrate the feasibility of the proposed approach, we present excerpts of a large-scale lifetime study on a large commercial 64 Ah NMC532/graphite pouch cell. Cell ageing at different temperatures (Section 3.1) was followed by conventional CC-ICA (Section 3.2). In Section 3.3, we compare several approaches for OCV estimation and look into varying both SoC resolution and relaxation times (Section 3.4), aiming to reduce the measurement time below the 40 h required for a full C/20 cycle, while still resolving the main electrode

features. Subsequently, we present a direct comparison of the obtained OCV-ICA and CC-ICA results in Section 3.5.

2. Materials and Methods

2.1. Data Collection

Cell type and setup. The cell used in this study was a large commercial 64 Ah pouch cell, with an NMC532/graphite chemistry. A total of over 140 cells were tested within a large-scale aging and safety study, and data from 18 cells were used specifically in this paper. The cells were tested under controlled environments in temperature chambers within voltage limits of 3 V and 4.2 V, according to the manufacturers' specifications. All cells were mounted in a mechanical fixture with 10 mm aluminum plates around the cell and a 1 Nm torque on the six 10 mm bolts. In addition, a 5 mm aluminum plate with a narrow groove was placed on top of the cell to accommodate a Pt-100 temperature sensor at the center of the pouch cell surface. The measurement setup is shown in Figure 2.

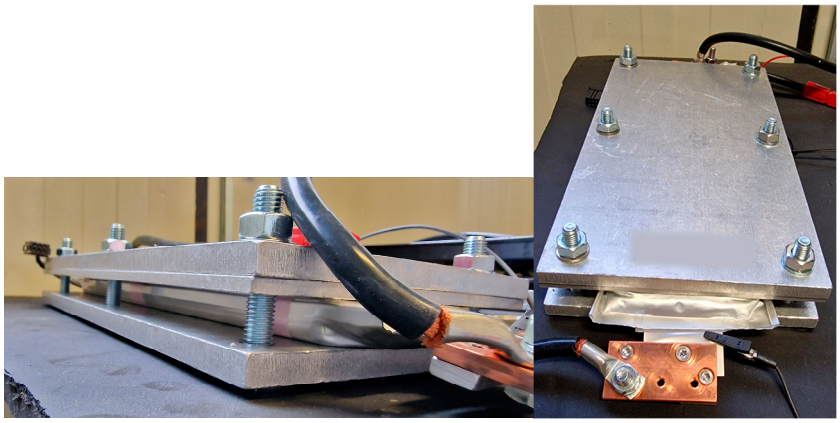

Figure 2. Measurement setup: pouch cell mounted in the mechanical fixture including clamps for current on the cell tab as well as voltage sense.

Cell cycling. All cycling was performed with battery testers from PEC, either SBT-0550 or ACT-0550 testers. The cells were kept in dedicated temperature-controlled chambers for the five selected test temperatures.

Cell characterization. All cells were initially characterized at 25 ± 1 °C employing a characterization protocol including 0.75 C, 0.25 C, and 0.05 C constant-current cycles. All charge steps were finished with a CV step at 4.2 V to reach 0.05 C. The characterization protocol included a high-power pulse-like test (HPPC) to unveil details of cell resistance and OCV in steps of 5% SoC, from 100% SoC to 0% SoC.

Ageing study. The presented dataset is part of a large-scale ageing study including cells aged at 5, 15, 25, 35, and 45 °C cycling from 0 to 100% SoC at 0.75 C current. A minimum of 5 min OCV between charge and discharge was required. If the cell temperature was (still) higher than 1 °C above the wanted cycling temperature, the cell was allowed to cool until the 1 °C limit was reached before the next charge or discharge was started. The initial cell characterization at 25 °C was repeated in regular intervals (after (i) a defined number of cycles or (ii) a total maximum test time or when (iii) the remaining capacity for the cycling protocol had dropped 5% during the cycling) until the cell reached its end of life at 80% SoH.

OCV measurements. The detailed pOCV curve was measured occasionally in significantly higher SoC resolution than in the standard HPPC test protocol. A current pulse of 0.5 C was used to discharge or charge the cell in SoC steps of 1% or less. The pOCV values were established by taking the value at t = 15 min after the end of the current pulse. To reduce the influence of noise in the data, this pOCV value was verified by direct comparison to a fitted exponential regression curve against the voltage relaxation data.

2.2. Data Handling

CC-ICA. Conventional CC-IC data were extracted from the C/20 data collected during the regular characterization cycles. The method for calculating dQ/dV from charge and discharge curves was described in detail in our earlier work [24]: "As the original voltage-versus-capacity curves contain measurement noise, it is necessary to apply a filtering algorithm to obtain the IC data. Since the number of data points per capacity step might be uneven, the measured voltages are averaged in capacity steps of 0.05% of the full capacity span. After averaging the dataset, a local second-order polynomial regression is fitted to the voltage as a function of capacity with a moving capacity window. The size of the moving capacity window is limited by either a voltage window (20 mV) or a capacity window (5%), whichever is the limiting variable".

OCV-ICA. OCV-IC data were established from the detailed OCV measurements described above, following the same smoothing methodology used for CC-ICA.

3. Results

3.1. Cycle Life

The cycling study included a total of 18 cells that were aged at five different temperatures. The results are summarized in Figure 3. We observed that cycling at temperatures above 25 °C reduced the cycle life. Cycling at 25 °C allowed for a cycle life of 3000 equivalent full cycles at 80% SoH, while the cycle life was reduced to 2100 EFC at 35 °C and even further down to 1450 EFC at 45 °C. Even though the cycle conditions at 5 °C exhibited a higher initial drop in capacity, cycling at 5 °C and 15 °C resulted in cycle lives of around 3000 EFC, comparable to those at 25 °C.

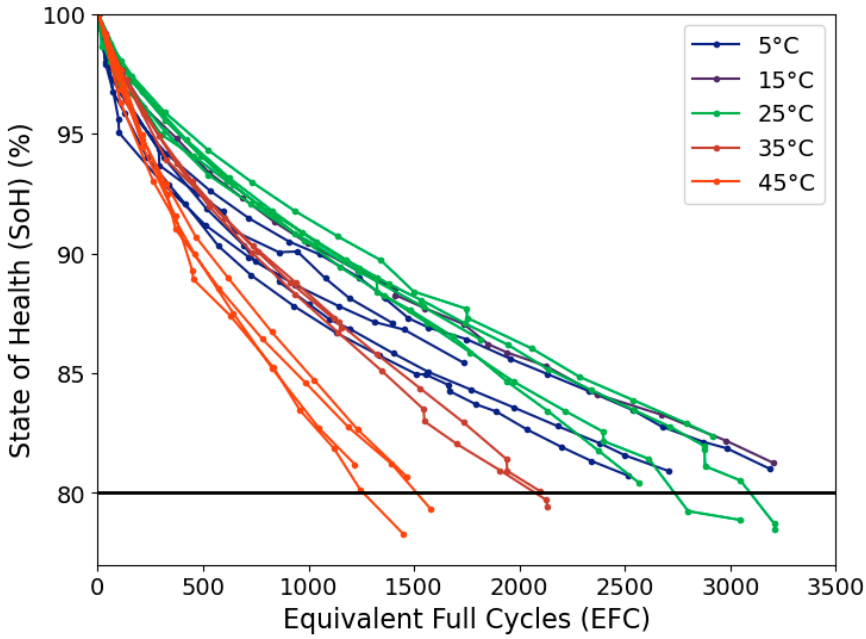

Figure 3. Cycle life for cells cycled at 0.75 C in the full SoC window at different temperatures.

Depending on the cycling conditions, the mechanisms leading to the observed loss in capacities can be quite different but cannot be inferred from a simple lifetime plot. A detailed ICA can allow for the extraction of more details of the underlying ageing mechanisms.

3.2. Qualitative Aging Diagnostics via ICA

Figure 4 shows the evolution of the IC curves throughout the life of a cell cycled at room temperature (25 °C). As the cell aged, we observed qualitative changes in the IC for both discharge (negative dQ/dV values) and charge (positive dQ/dV values). In the IC at 100% SoH, on charging, we observed two large peaks at 3.49 V and 3.645 V, while a local

minimum (valley) was observed at 3.765 V as well as some smaller peaks around 3.6 V. These peaks stemmed from the phase transitions of graphite during lithiation as well as from changes within the NMC material during de-lithiation, as elaborated by Spitthoff [24]. The positions of these changes during the ageing progression significantly depend on the dominating ageing modes.

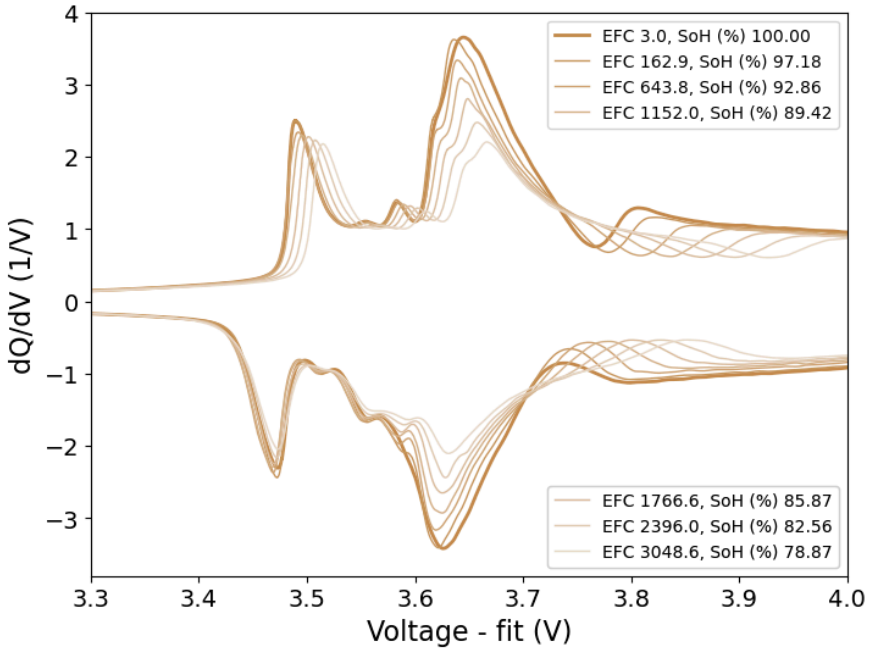

Figure 4. Evolution of dQ/dV for a cell cycled at 25 °C from 100% to 80% SoH.

To illustrate the influence of temperature on the degradation pathways, Figures 5 and 6 show the corresponding IC curves at 5 and 45 °C. It can clearly be seen that even at similar SoH, the features of the IC curves evolved in different ways, pointing towards different types of degradation mechanisms. For a more thorough interpretation of those curves, including a more detailed and quantitative analysis, refer to our previous work [24].

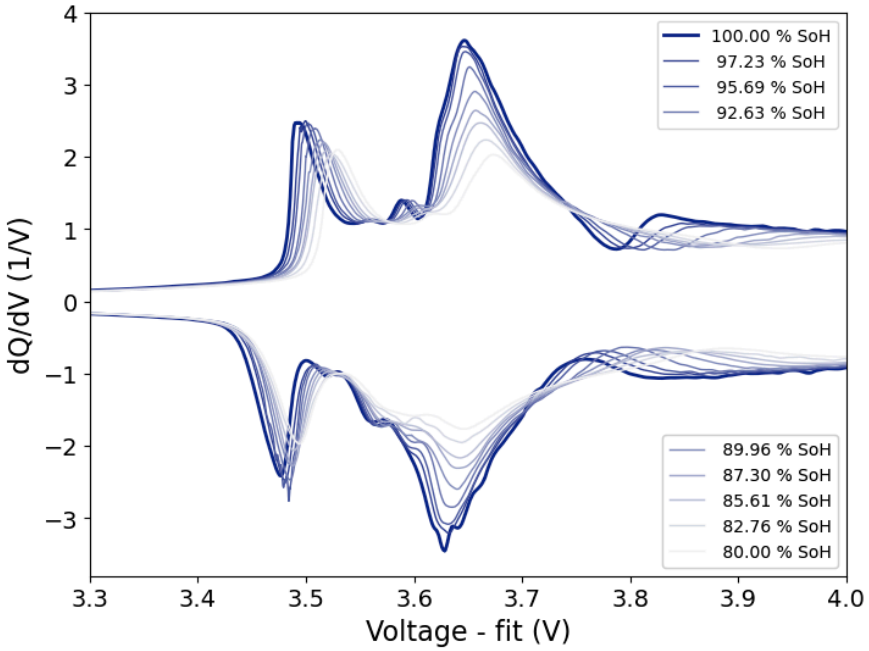

Figure 5. Changes in dQ/dV for cells aged at 5 °C from 100% to 80% SoH.

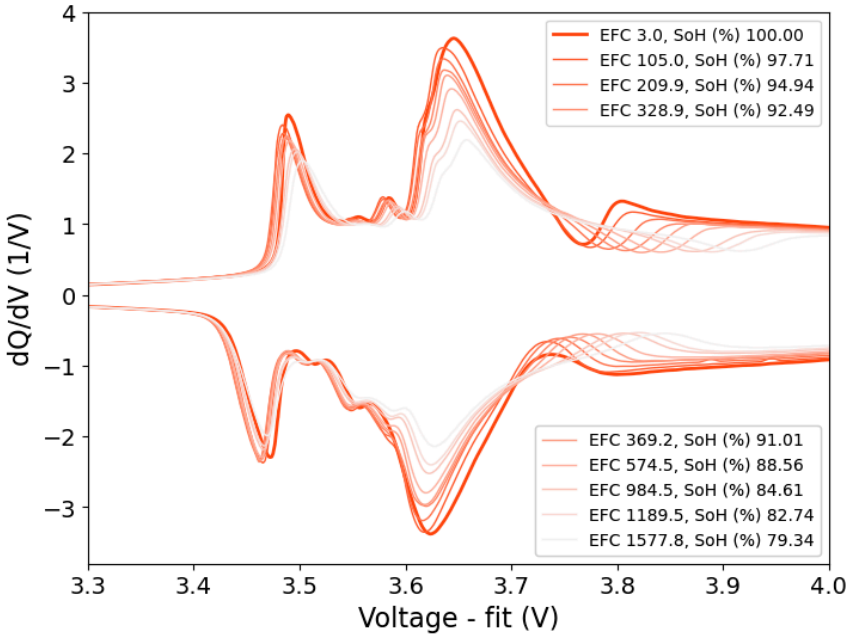

Figure 6. Changes in dQ/dV for cells aged at 45 °C from 100% to 80% SoH.

3.3. Measurement of OCV Curves

Two basic approaches are commonly employed to approximate the "true" OCV curve: slow CC charge and discharge as well as pulsing protocols with varying relaxation times and SoC steps. To evaluate the different approaches with respect to their applicability for ICA, several different measurements were performed. Figure 7 shows the direct comparison of a representative selection of measured pOCV curves, including charge and discharge curves for C/20 and C/100 as well as a pOCV curve obtained by employing 0.5 C current pulses in 0.5% SoC steps and with 15 min relaxation times.

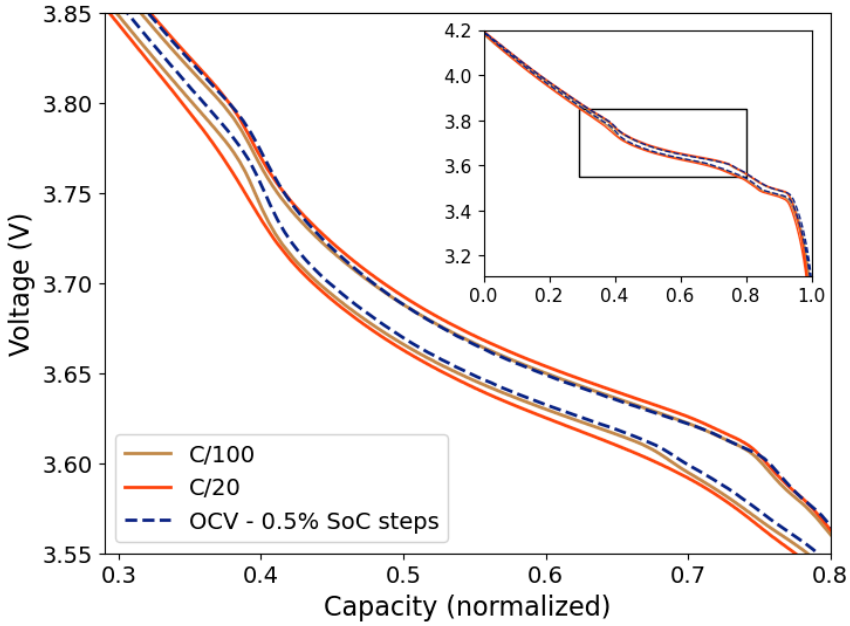

Figure 7. Direct comparison of C/20, C/100, and current-pulse pOCV curves.

The observed hysteresis between charge and discharge got smaller with decreasing C-rates and thus closer to the actual equilibrium voltage. The voltage hysteresis for the current-

pulse protocol was even smaller than for the slow constant-current cycles, indicating an even better approximation to the "true" OCV.

3.4. Influence of the Pulsing Parameters on the OCV-IC Curves

To better resolve the features of the pOCV curves and evaluate similarities and differences between slow CC and pulsing approaches, the corresponding dQ/dV curves were analyzed. As a first step, we took a closer look at the influence of the pulsing parameters on the resulting pOCV curve as well as on their effects on the resulting dQ/dV curves. It should be noted that OCV curves based on constant current can never be denoted as "actual" OCV curves, since the cell is not at an OCV equilibrium but has a small polarization shift proportional to the actual current. This polarization causes a voltage shift of the IC curve proportional to the applied current, and the shift accumulates over the SoC and, hence, is not constant throughout the obtained IC curves.

OCV-IC data were obtained from the pOCV curves using a variety of different pulsing protocols. The influence of the selected influential pulsing parameters (relaxation times and SoC resolution) on the resulting dQ/dV curves was investigated.

Relaxation times. The relaxation time after a current pulse determines how close one gets to the "true" OCV. Figure 8 shows the influence of selected relaxation times on the resulting dQ/dV curves. Even short relaxation times of 5 min showed peak shifts smaller than those observed for the CC-IC curves, despite comparably high current pulses of 0.5 C. The OCV-IC curves seemed to stabilize for relaxation times larger than 15 min, with very similar IC curves at both 15 and 30 min of relaxation time. Thus, 15 min seemed to be a good experimental compromise with respect to a maximum necessary relaxation time for this cell. Some noise in the IC signals was observed, especially for the first peaks around 3.47 V. This can most likely be attributed to the applied smoothing algorithm that was not (yet) fully optimized for the significantly smaller number of datapoints across the SoC window used for obtaining the OCV-IC curves compared to that used for the CC-IC curves (see below).

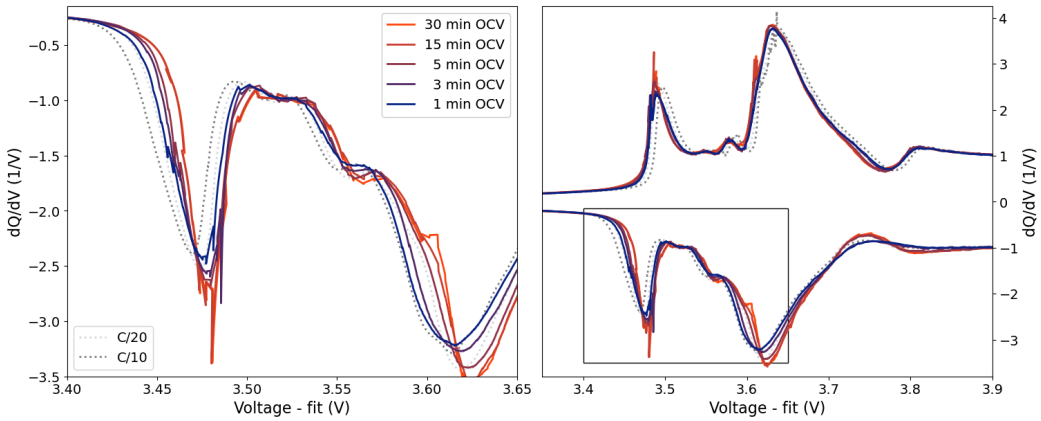

Figure 8. Influence of the relaxation times on the resulting OCV-dQ/dV. Left: zoom into the selected region marked on the right.

SoC resolution. The SoC resolution of the pulsing protocols significantly affected the quality of the obtained OCV-IC data. A SoC resolution of 2% (50 steps) was enough to resolve the main IC features, while a SoC resolution of 0.5% (200 steps) properly resolved even small features (Figure 9). SoC-dependent resolution adjustments around areas of interest could further reduce the necessary number of steps. Note that the smoothing algorithm settings could affect the actual outcome of the ICA and had to be further optimized, specifically with respect to OCV-ICA.

Based on the discussion above, in the following, we used the pOCV dataset with a 15 min relaxation time and a SoC resolution of 1%.

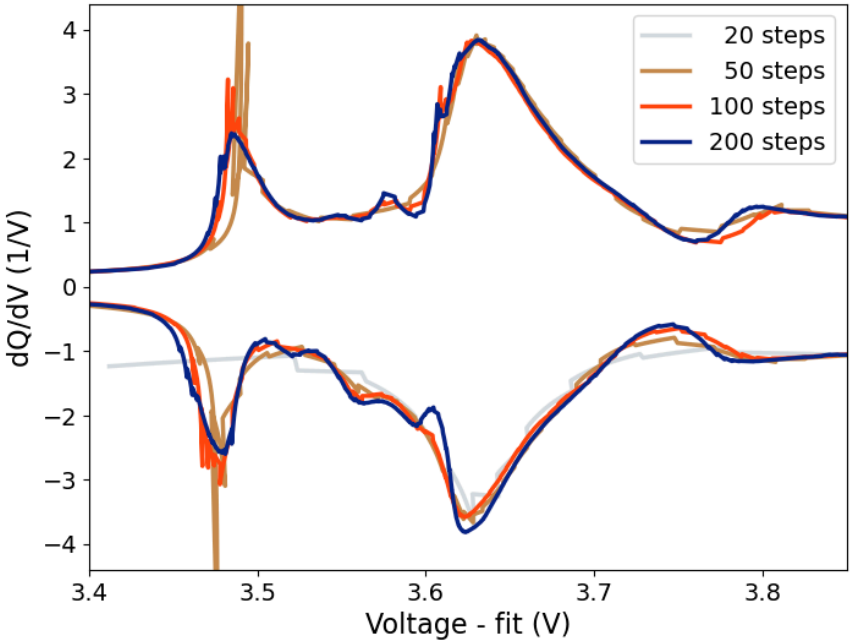

Figure 9. Influence of SoC resolution on the resulting OCV-dQ/dV curves.

3.5. Direct Comparison of CC-ICA and OCV-ICA

To evaluate the diagnostic capability of OCV-ICA versus conventional CC-ICA, a direct comparison was performed for cells aged to 80% SoH at both 5 and 45 °C. The results are shown in Figure 10. The dQ/dV values from both approaches showed very similar patterns for both new and aged cells. All main features were preserved with OCV-ICA. The shifts in voltage between the CC-IC and OCV-IC curves were caused by the small polarization at low constant currents. This shift could increase through ageing and due to an increase in internal resistance; however, for this specific cell, the increase in internal resistance upon ageing was low [24]. These results provide a proof of concept for using OCV-ICA as a diagnostic tool similar to CC-ICA.

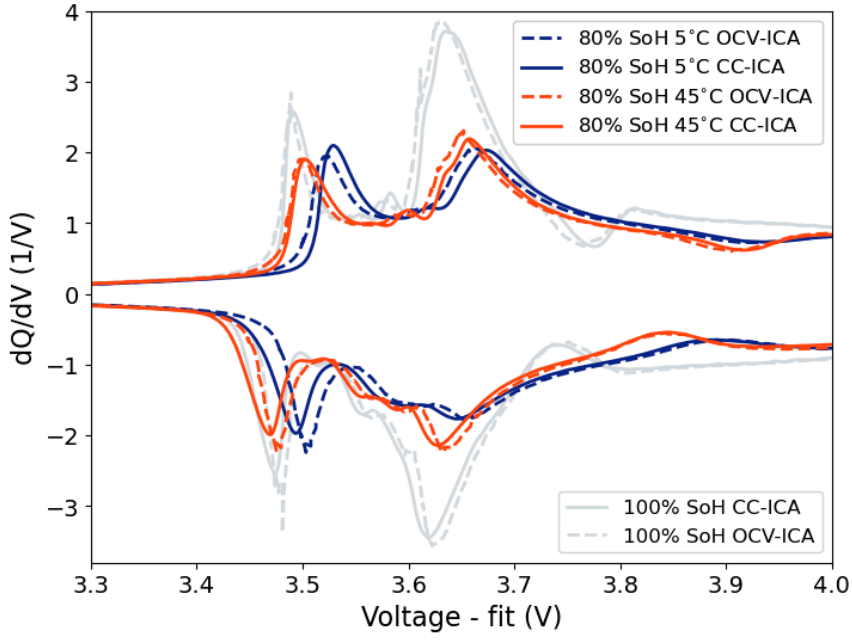

Figure 10. Direct comparison of CC-ICA and OCV-ICA at 100% SoH (grey) and 80% SoH for cells aged at 5 °C (blue) and 45 °C (red).

4. Discussion

This work introduces the concept of OCV-ICA as a potential diagnostic tool and presents a proof of concept for the feasibility and applicability of OCV-ICA as an alternative to CC-ICA. OCV-ICA offers two main advantages over classical CC-ICA: (1) the possibility to obtain diagnostic information on battery systems without a significant interruption of normal cell operation; (2) the potential for a significant reduction in the measurement time upon proper optimization of the measurement conditions.

Using an excerpt of a large-scale cycle-life study at three different temperatures, we investigated and directly compared the diagnostic capabilities of OCV-ICA and CC-ICA, as well as the influence of selected parameters onto the results. The results presented in Figure 10 clearly illustrate the main features and trends for cells aged under different conditions, reproduced in the IC curves obtained from pOCV data. The main noticeable difference is the voltage shift due to polarization during CC for the CC-IC curves.

Potential for a reduction in the measurement time. While the "true" OCV at any SoC is assumed to be reached only after a long relaxation time of several hours, resulting in very time-consuming experiments (see Table 1), the presented results (Figure 8) illustrate that for OCV-ICA, it is not the absolute "true" OCV curve that matters, but there is a minimum required relaxation time resulting in a "good-enough" OCV-ICA curve. This opens a range of possibilities for further optimizing the relaxation times while minimizing the total measurement time, including, e.g., the investigation of SoC-dependent relaxation times as well as the extrapolation of the initial relaxation times to a standard relaxation time of, e.g., 60 min. The presented examples of relaxation times and their influence on the resulting IC curves (Figure 8) illustrated that even relaxation times as short as 15 min per SoC step gave comparable IC curves as the longer 30 min relaxation. Even the 5 min relaxation time gave a consistently lower voltage shift than observed for the conventional CC-IC curves.

Table 1. Comparison of estimated test time for an OCV-ICA test with 0.5 C pulse current with different OCV relaxation times and SoC resolution for both charge and discharge with those for CC-ICA tests with 0.05 and 0.01 C current.

Test Type	SoC Resolution (%)	OCV Time (min)	Total Test Time (days)
OCV	1	1	0.3
OCV	1	3	0.6
OCV	1	5	0.9
OCV	1	15	2.3
OCV	1	30	4.3
OCV	0.5	1	0.4
OCV	0.5	5	1.6
OCV	0.5	15	4.3
OCV	0.5	30	8.5
OCV	0.5	60	16.8
CC-0.05 C			1.7
CC-0.01 C			8.3

Similarly, the measurement time can be reduced by reducing the number of measurement points across the SoC window. The influence of SoC resolution on the quality of the obtained OCV-IC curves is illustrated in Figure 9. While a sufficiently high SoC resolution is required across highly predictive features intended to be used for subsequent diagnostic analysis, a reduction in SoC resolution seems feasible across SoC ranges showing lower variation in dQ/dV.

The total test times for the selected parameters for both OCV-IC and CC-IC data collections are summarized in Table 1. We observed that, e.g., a 5 min relaxation with 1% SoC steps could be measured in less than 24 h, while the conventional 0.05 C CC-IC tests took at least 40 h (exhibiting a larger voltage shift).

In addition to the preliminary experiments presented here, there is a large literature base on establishing methods for high-precision SoC estimation based on the reconstruction of OCV [20–22]. These pOCV curves are applied to BMSs for improved SoC estimation. By learning from these methods, OCV-IC curves may be measured even faster.

Within standard cell testing using high-accuracy equipment in the laboratory, CC-ICA may still be superior due to the high sampling rate and, consequently, very high data resolution across the entire SoC range. However, the longer measurement times for performing a full high-quality CC-ICA of more than 40 h at a low 0.05 C current and the possibility to significantly reduce this time make OCV-ICA a viable addition for diagnostic data collection also in laboratory environments.

Application-friendly diagnostics. However, the main benefits of OCV-ICA can be exploited outside of high-precision laboratory environments where a constant current is challenging to obtain. Any current pulse, either constant current or power, and the following OCV relaxation can yield a pOCV measurement point that can then be accumulated into an pOCV curve usable for OCV-ICA. Provided the voltage resolution within a system's BMS is sufficiently high, individual OCV-IC curves can then be achieved for any local cell parallel within the module or pack. This allows for exploiting the natural breaks within a battery system's operational profile. By collecting these randomized "natural" pOCV points across a necessary time period (i.e., one week), a "complete" pOCV curve with the required resolution for subsequent OCV-ICA can be obtained (Figure 1). This can enable the possibility to extract online diagnostic information on every cell parallel in a battery system without operational interruption.

Supplementary Materials: The following supporting information can be downloaded at: https://www.mdpi.com/article/10.3390/batteries10080277/s1, This includes .csv of differently obtained OCV curves, .csv of selected dQ/dV curves, and .csv of lifetime data.

Author Contributions: Conceptualization, J.W. and P.J.S.V.; experiments and formal analysis, P.J.S.V.; visualization, J.W.; writing—original draft, review and editing, J.W. and P.J.S.V. All authors have read and agreed to the published version of the manuscript.

Funding: The authors acknowledge the Research Council of Norway and partner companies of the projects BattMarine (Grant No. 281005), MoreIsLess (Grant No. 324077), and 2ND LIFE (Grant No. 320760) for financial support.

Data Availability Statement: The original data presented in the study are included in the article's Supplementary Material; further inquiries can be directed to the corresponding author.

Acknowledgments: Jan Petter Mæhlen is acknowledged for making Figure 1.

Conflicts of Interest: The authors declare no conflicts of interest. The funders had no role in the design of the study; in the collection, analyses, or interpretation of data; in the writing of the manuscript; or in the decision to publish the results.

References

1. Chen, T.M.; Jin, Y.; Lv, H.Y.; Yang, A.T.; Liu, M.Y.; Chen, B.; Xie, Y.; Chen, Q. Applications of Lithium-Ion Batteries in Grid-Scale Energy Storage Systems. *Trans. Tianjin Univ.* **2020**, *26*, 208–217. [CrossRef]
2. He, W.; Mo, O.; Remoy, A.; Valoen, L.O.; Satendal, H.; Howie, A.; Vie, P.J.S. Accelerating Efficient Installation and Optimization of Battery Energy Storage System Operations Onboard Vessels. *Energies* **2022**, *15*, 4908. [CrossRef]
3. Lian, T.; Vie, P.J.S.; Gilljam, M.; Forseth, S. (Invited) Changes in Thermal Stability of Cyclic Aged Commercial Lithium-Ion Cells. *ECS Trans.* **2019**, *89*, 73–81. [CrossRef]
4. Dubarry, M.; Ansean, D. Best practices for incremental capacity analysis. *Front. Energy Res.* **2022**, *10*, 18. [CrossRef]
5. Ratnakumar, B.V.; Smart, M.C. Lithium Plating Behavior in Lithium-ion Cells. In *Rechargeable Lithium-Ion Batteries*; Winter, M., Doughty, D.H., Zaghib, K., Abraham, K.M., Ogumi, Z., Dudney, N.J., Eds.; Electrochemical Soc Inc.: Pennington, SA, USA, 2010; Volume 25, pp. 241–252.
6. Smith, A.J.; Fang, Y.; Mikheenkova, A.; Ekstrom, H.; Svens, P.; Ahmed, I.; Lacey, M.J.; Lindbergh, G.; Furo, I.; Lindstrom, R.W. Localized lithium plating under mild cycling conditions in high-energy lithium-ion batteries. *J. Power Sources* **2023**, *573*, 15. [CrossRef]

7. Cabrera-Castillo, E.; Niedermeier, F.; Jossen, A. Calculation of the state of safety (SOS) for lithium ion batteries. *J. Power Sources* **2016**, *324*, 509–520. [CrossRef]
8. Barai, A.; Uddin, K.; Dubarry, M.; Somerville, L.; McGordon, A.; Jennings, P.; Bloom, I. A comparison of methodologies for the non-invasive characterisation of commercial Li-ion cells. *Prog. Energy Combust. Sci.* **2019**, *72*, 1–31. [CrossRef]
9. Goldammer, E.; Kowal, J. Investigation of degradation mechanisms in lithium-ion batteries by incremental open-circuit-voltage characterization and impedance spectra. In Proceedings of the 17th IEEE Vehicle Power and Propulsion Conference (VPPC), Virtual, 18 November–16 December 2020.
10. Yin, L.T.; Geng, Z.Y.; Chien, Y.C.; Thiringer, T.; Lacey, M.J.; Andersson, A.M.; Brandell, D. Implementing intermittent current interruption into Li-ion cell modelling for improved battery diagnostics. *Electrochim. Acta* **2022**, *427*, 12. [CrossRef]
11. Dubarry, M.; Svoboda, V.; Hwu, R.; Liaw, B.Y. Incremental capacity analysis and close-to-equilibrium OCV measurements to quantify capacity fade in commercial rechargeable lithium batteries. *Electrochem. Solid. State Lett.* **2006**, *9*, A454–A457. [CrossRef]
12. Olson, J.Z.; López, C.M.; Dickinson, E.J.F. Differential Analysis of Galvanostatic Cycle Data from Li-Ion Batteries: Interpretative Insights and Graphical Heuristics. *Chem. Mat.* **2023**, *35*, 1487–1513. [CrossRef]
13. Takano, K.; Saito, Y.; Kanari, K.; Nozaki, K.; Kato, K.; Negishi, A.; Kato, T. Entropy change in lithium ion cells on charge and discharge. *J. Appl. Electrochem.* **2002**, *32*, 251–258. [CrossRef]
14. Devie, A.; Dubarry, M.; Liaw, B.Y. Diagnostics of Li-Ion Commercial Cells–Experimental Case Studies. In Proceedings of the Symposium on Lithium-Ion Batteries Held during the 224th Meeting of the Electrochemical-Society (ECS), San Francisco, CA, USA, 27 October–1 November 2013; pp. 193–205.
15. Dubarry, M.; Liaw, B.Y. Identify capacity fading mechanism in a commercial $LiFePO_4$ cell. *J. Power Sources* **2009**, *194*, 541–549. [CrossRef]
16. Liu, P.; Wu, Y.Z.; She, C.Q.; Wang, Z.P.; Zhang, Z.S. Comparative Study of Incremental Capacity Curve Determination Methods for Lithium-Ion Batteries Considering the Real-World Situation. *IEEE Trans. Power Electron.* **2022**, *37*, 12563–12576. [CrossRef]
17. Schaltz, E.; Stroe, D.I.; Norregaard, K.; Ingvardsen, L.S.; Christensen, A. Incremental Capacity Analysis Applied on Electric Vehicles for Battery State-of-Health Estimation. *IEEE Trans. Ind. Appl.* **2021**, *57*, 1810–1817. [CrossRef]
18. Petzl, M.; Danzer, M.A. Advancements in OCV Measurement and Analysis for Lithium-Ion Batteries. *IEEE Trans. Energy Convers.* **2013**, *28*, 675–681. [CrossRef]
19. Dubarry, M.; Baure, G. Perspective on Commercial Li-ion Battery Testing, Best Practices for Simple and Effective Protocols. *Electronics* **2020**, *9*, 152. [CrossRef]
20. Blanc, J.; Schaeffer, E.; Auger, F.; Diab, Y.; Cousseau, J.F. A new time-adjustable model-based method for fast open-circuit voltage estimation of Lithium-ion cells. *J. Power Sources* **2023**, *586*, 12. [CrossRef]
21. Zhou, M.Y.; Zhang, J.B.; Ko, C.J.; Chen, K.C. Precise prediction of open circuit voltage of lithium ion batteries in a short time period. *J. Power Sources* **2023**, *553*, 11. [CrossRef]
22. Birkl, C.R.; McTurk, E.; Roberts, M.R.; Bruce, P.G.; Howey, D.A. A Parametric Open Circuit Voltage Model for Lithium Ion Batteries. *J. Electrochem. Soc.* **2015**, *162*, A2271–A2280. [CrossRef]
23. Prosser, R.; Offer, G.; Patel, Y. Lithium-Ion Diagnostics: The First Quantitative In-Operando Technique for Diagnosing Lithium Ion Battery Degradation Modes under Load with Realistic Thermal Boundary Conditions. *J. Electrochem. Soc.* **2021**, *168*, 14. [CrossRef]
24. Spitthoff, L.; Vie, P.J.S.; Wahl, M.S.; Wind, J.; Burheim, O.S. Incremental Capacity Analysis (dQ/dV) as a Tool for Analysing the Effect of Ambient Temperature and Mechanical Clamping on Degradation. *J. Electroanal. Chem.* **2023**, *944*, 117627. [CrossRef]